Electronic Supplementary Material (ESI) for Journal of Materials Chemistry A.


**Supporting Information**

# 3D printing of Fe-based Bulk Metallic Glass and Composite Components with Large Dimensions and Enhanced Toughness by Thermal Spraying

Cheng Zhang[1, a], Wei Wang[1, a], Yi-Cheng Li[a], Yan-Ge Yang[b], Yue Wu[c] and Lin Liu[a, *]

[a]The State Key Lab for Materials Processing and Die & Mould Technology, School of Materials Science and Engineering, Huazhong University of Science and Technology, #1037, Luo Yu road, 430074Wuhan, China.

[b] Laboratory for Corrosion and Protection, Institute of Metal Research, Chinese Academy of Sciences, No. 62 Wen cui Road, 110016 Shenyang, China.

[c]Department of Physics and Astronomy, University of North Carolina, Chapel Hill, NC 27599-3255, USA.

*Corresponding author. E-mail: lliu2000@mail.hust.edu.cn

[1] Cheng Zhang and Wei Wang contributed equally to this work.

**Microstructure characterization of the TS3DP-BMG, TS3DP-BMGC and as-cast BMG**

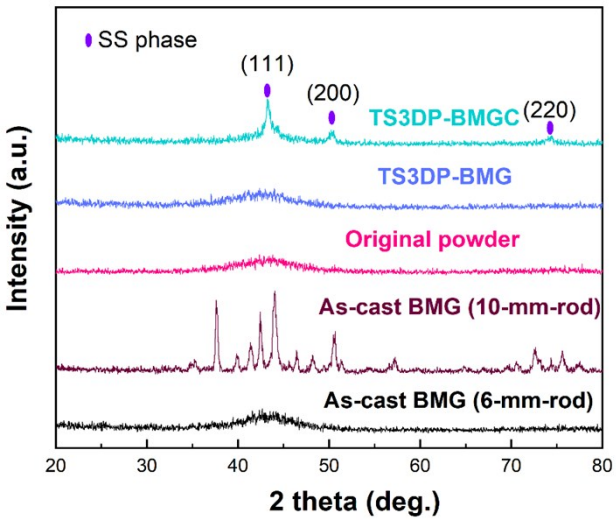


**Figure S1.** XRD patterns of the TS3DP-BMG and TS3DP-BMGC (with 50wt% 316L SS), as compared to the original amorphous powder and as-cast $Fe_{48}C_{15}B_6Mo_{14}Cr_{15}Y_2$ BMG rods with a diameter of 6 mm and 10 mm.

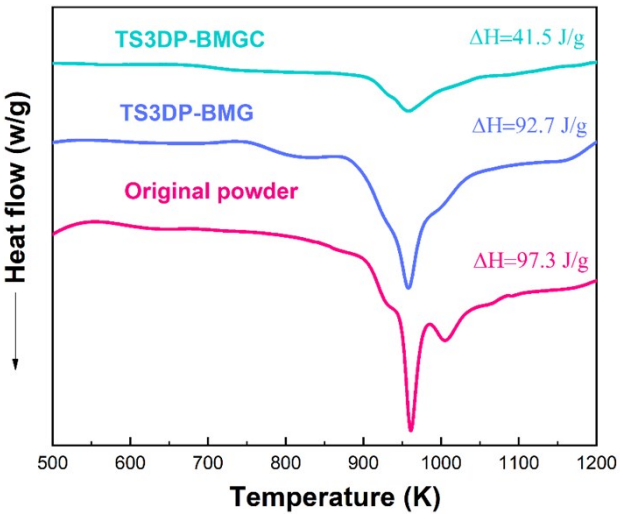


**Figure S2**. Differential thermal analysis (DTA) plots of the TS3DP-BMG and TS3DP-BMGC samples as compared to the original powders. Taking the crystallization enthalpy of the original powder as the base, the fraction of amorphous phase in the TS3DP-BMG and TS3DP-BMGC samples can be calculated according to the change in the enthalpy, e.g., $\chi$(amorphous fraction)=$\Delta H_{\text{TS3DP-sample}}/\Delta H_{\text{powder}}$, which yields approximately 95% and 43% amorphous phase in the TS3DP-BMG and TS3DP-BMGC samples.

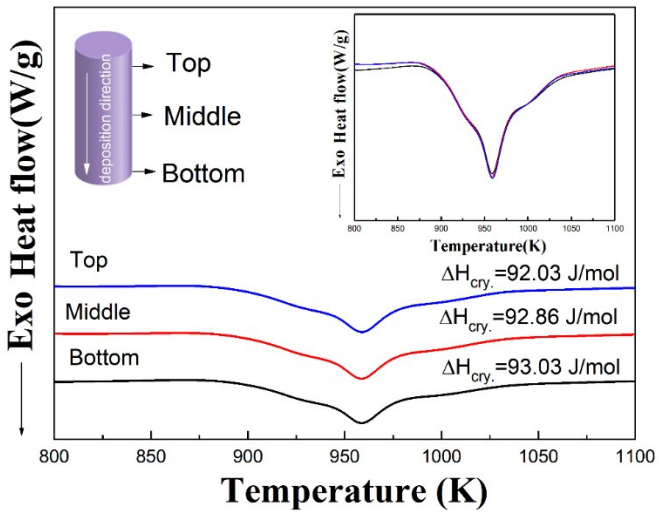


**Figure S3**. Differential thermal analysis (DTA) plots taken from different regions (top, middle and bottom) of a 3-mm-rod TS3DP-BMG sample. Inset shows the three DTA curves are similar with the same crystalline temperature and exothermic reaction, confirming that each deposited layer have a similar amorphous structure. The bottom region means ~1 mm perpendicularly away from the substrate; while the bottom region is ~1 mm perpendicularly away from the surface.

**Alternating hard/soft structure in the TS3DP-BMGC sample by microhardness measurement**

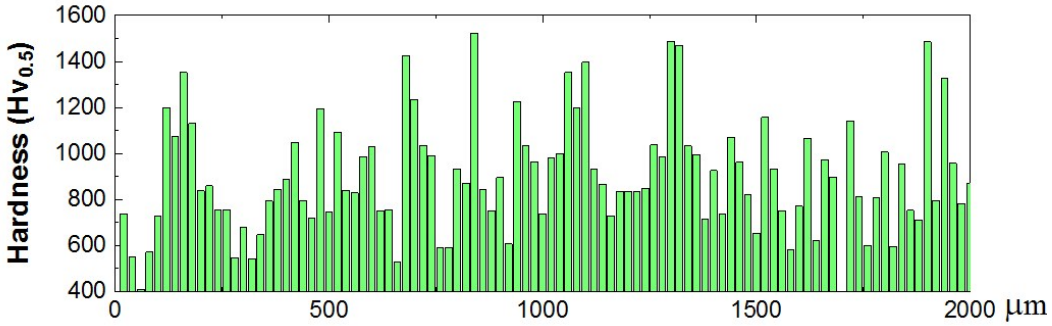


**Figure S4**. Microhardness distribution in the TS3DP-BMGC sample showing the alternating hard and soft structure.

The microhardness was measured using a micro-indenter with the load of 50 g and a dwell time of 15 s. To obtain the microhardness distribution in the TS3DP-BMGC specimen, we took the hardness measurements along the deposition direction across a 2000-μm distance with a constant interval of 20 μm between each indentation. The result shown in Fig. S4 clearly demonstrate the

structure with alternating soft and hard regions in the TS3DP-BMGC specimen, which could be effective in hindering the crack prorogation.

**Fracture toughness assessment based upon surface roughness analysis**

The fraccture toughness was assessed according to the method proposed by Kotoul *et al*. [1]. Basically, a simple pyramidal model of the crack front was proposed for approximate analytical estimations, in which the tortuous crack front is characterized by the title angle (Ø) and twist angle ($\Theta$) towards the macroscopic crack plane, as illustrated in **Figure S5**.

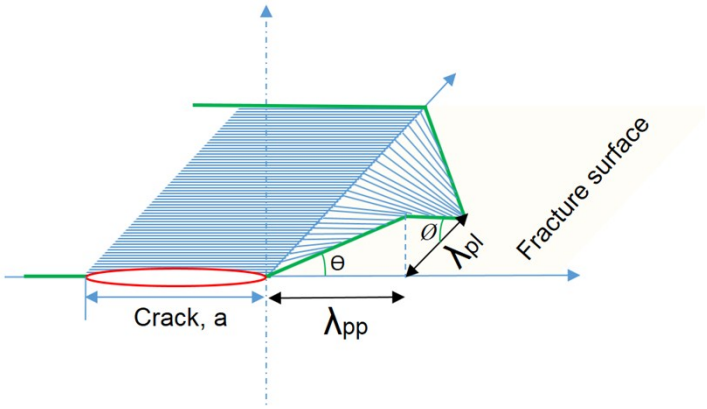


**Figure S5**. Scheme of the pyramidal model approximating the tortuous crack front.

The two angles are associated with the profile roughness ($R_L$, measured along the crack front), and the profile periodicity $\lambda_{pp}$ and $\lambda_{pl}$ measured parallel and perpendicular to the crack front, by the following equations:

$$\lambda_{pp} \tan \Theta = \lambda_{pl} \tan \text{Ø} \quad (1)$$

$$R_L = \cos^{-1} \text{Ø}, \quad (2)$$

The $\lambda_{pp}$ and $\lambda_{pl}$ are determined by the Fourier analysis of the roughness profiles measured on the fracture surface. The measured values for the TS3DP-BMG, TS3DP-20BMGC, TS3DP-50BMGC and as-cast samples are summarized in **Table S1**.

Based on the data obtained, the effective stress intensity factor $k_{eff}$ for the pyramidal model of the crack front was then calculated as:

$$k_1 = \cos(\Theta/2)[2v \sin^2 \text{Ø} + \cos^2(\Theta/2)\cos^2 \text{Ø}] \quad (3)$$

$$k_2 = \sin(\Theta/2) \cos^2(\Theta/2) \quad (4)$$

$k_3=\cos(\Theta/2)\sin\Phi\cos\Phi\,[2\nu-\cos^2(\Theta/2)]$ (5)

$$k_{eff}^2=\frac{\pi-2}{2\Theta(2R_L+\pi-4)}\int_{-\Theta}^{\Theta}\left(k_1^2+k_2^2+\frac{k_3^2}{1-\nu}\right)d\Theta \quad (6)$$

Then, the predict fracture toughness ($K_{IC}$) was calculated using the following equation:

$$\frac{K_{IC}}{K_{IMC}}=\frac{1}{k_{eff}} \quad (7)$$

where $K_{IMC}$ represents the fracture toughness of undeflection sample, i.e., as-cast BMG in the present study. The calculated ratio between $K_{IC}$ and $K_{IMC}$ are shown in **Table S1**.

**Table S1**. Characteristics of the pyramidal model related to the measured samples

| Samples | $R_L$ | $\lambda_{pp}$ (μm) | $\lambda_{pl}$ (μm) | $\Phi$ | $\Theta_m$ | $k_{eff}$ | $K_{IC}/K_{IMC}$ |
|---|---|---|---|---|---|---|---|
| As-cast BMG | 1.04 | 230 | 236 | 0.28 | 0.29 | 0.94 | 1.07 |
| TS3DP-BMG | 1.64 | 270 | 242 | 0.91 | 0.86 | 0.52 | 1.92 |
| TS3DP-BMGC | 4.42 | 199 | 418 | 1.34 | 1.46 | 0.24 | 4.17 |

**Supporting references**

[1] M. Kotoul, J. Pokluda, P. Sandera, I. Dlouhy, Z. Chlup, A.R. Boccaccini, **Acta Mater.**, 2008, 56, 2908.